ELSEVIER

Catalysis Today 70 (2001) 359–368

CATALYSIS TODAY

www.elsevier.com/locate/cattod

Flow-mediated spatial coupling during CO oxidation on a palladium-supported catalyst in a continuous-flow reactor

A. Ohlhoff [a], H. Engel [b,*]

[a] *Center of Applied Space Technology and Microgravity (ZARM), University of Bremen, Am Fallturm, D-28359 Bremen, Germany*
[b] *Institut für Theoretische Physik, Technische Universität Berlin, Hardenbergstrasse 36, D-10623 Berlin, Germany*

Abstract

We consider the CO oxidation in a continuous-flow reactor containing *N* catalytic layers of zeolite-supported palladium. For the kinetics of the reaction in one layer, we adopt a model proposed by Slin'ko and Jaeger. Rather than studying non-uniform coverage patterns on the individual catalyst layers, we focus on the influence of flow-mediated spatial coupling between the layers provided by variations in the CO partial pressure, which are transmitted by the flow to the adjacent downstream layer. Using the flow rate and the CO partial pressure at the inlet of the reactor as bifurcation parameters, in a parameter range where the reaction in one layer exhibits relaxational rate oscillations, we find different modes of operation for the reactor. The bifurcation diagram for two layers exhibits synchronized behavior at large flow rate. At lower flow rate and small CO partial pressure, we obtain a drop of catalytic activity at the first layer followed by a compensating increase at the second layer. In the multi-layer system, an increasing number of layers works synchronously when the flow rate grows up. Then, downstream and upstream moving pulse trains of catalytic activity can develop.

Keywords: CO oxidation; Pattern formation

1. Introduction

Spatio-temporal patterns in heterogeneous catalytic systems are prominent examples for spontaneous, self-organized formation of structures in macroscopic systems far from thermodynamic equilibrium [1]. Examples include coverage patterns observed on single crystal surfaces under ultra-high vacuum conditions [2,3], as well as spatio-temporal patterns in high-pressure catalytic reactors [4–6].

The mathematical modeling of this pattern formation is based on reaction–diffusion equations, describing the non-linear reaction kinetics and a local spatial coupling due to diffusion and/or heat conduction. The coupling between non-linear kinetics and diffusion is known to induce a wide spectrum of spatio-temporal patterns in chemical systems [7]. In catalytic reactors, external control is often applied to spatially averaged properties. Thermal patterns in high-pressure reactors, e.g., usually emerge due to a global constraint [6]. Global coupling through the gas phase has been shown to induce very complex spatio-temporal dynamics during reactions on catalytic surfaces [8–15]. Reacting species flowing at different flow rates may cause additional pattern formation as has been pointed out by Rovinsky and Menzinger [16,17] studying differential flow induced chemical instabilities. Altogether, catalytic systems admit several unique features as non-local spatial interaction, thermokinetic and convective instabilities, external feedback loops, etc.,

* Corresponding author. Tel.: +49-30-314-79462; fax: +49-30-314-21130.
E-mail address: h.engel@physik.tu-berlin.de (H. Engel).

0920-5861/01/$ – see front matter
PII: S0920-5861(01)00343-1

which must be taken into account for an adequate modeling. Thus, depending on the experimental situation, the mathematical models should be an extension from the classic reaction–diffusion models.

CO oxidation on a supported palladium catalyst is one of the best studied examples of oscillatory phenomena in heterogeneous catalytic systems [5,18–21]. Based on the reversible formation of subsurface oxygen and the Langmuir–Hinshelwood mechanism of catalytic CO oxidation, a kinetic model for this reaction was developed by Bassett and Imbihl [19], which explains the occurrence of rate oscillations. The model describes the elementary steps of adsorption, desorption and reaction between adsorbed carbon monoxide (CO_{ad}), adsorbed oxygen (O_{ad}), and subsurface oxygen (O_{sub}). Later on, this model was further modified by Slin'ko et al. [21] including a reaction of adsorbed CO with subsurface oxygen.

In this paper, we consider a continuous-flow reactor with N catalytic layers and focus on the interaction between the layers mediated by the flow through which the reactants are supplied. Variations in the CO partial pressure are transmitted downstream by the flow, while upstream communication is excluded. The question we would like to study is the following: if each layer can exhibit relaxation oscillations, what dynamic regimes are possible for the reactor. In Section 2, we extend the kinetic model discussed by Slin'ko et al. [21] in such a way that it accounts for a flow-mediated coupling between the catalytic layers in the reactor. In Section 3, we study the dynamic behavior of the extended model. We conclude with a short discussion of the main results.

2. The model

We consider a flow reactor with N catalytic layers perpendicular to the direction of the flow at a distance $d^{(j)}$ between the jth and the $(j+1)$th layer. The reactor geometry is schematically described in Fig. 1. Further experimental details are outlined in the paper by Slin'ko et al. [22]. For the kinetics of the reaction, we adopt the model formulated by Bassett and Imbihl [19], which was later on modified by Slin'ko and Jaeger (for a detailed discussion, see [21]). According to this model, the local concentration of adsorbed carbon monoxide (u), adsorbed oxygen (v), and subsurface oxygen (w) change with time as follows:

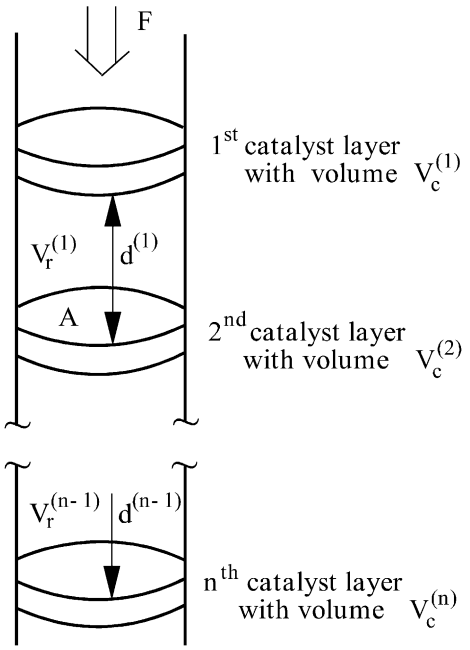

Fig. 1. Schematic sketch of the reactor. F: flow rate, A: cross-section of the reactor, $d^{(j)}$: distance and $V_r^{(j)} = d^{(j)}A$: volume between the jth and the $(j+1)$th layer.

$$\frac{du}{dt} = k_1 p_{CO}(1 - u - \delta v) - k_{-1}u - k_3 uv - k_5 uw, \tag{1}$$

$$\frac{dv}{dt} = k_2 p_{O_2} \exp(-\alpha w)(1 - u - v)^2 - k_3 uv - k_4 v(1 - w), \tag{2}$$

$$\frac{dw}{dt} = k_4 v(1 - w) - k_5 uw. \tag{3}$$

The terms in the first equation describe adsorption of CO from the gas phase, CO desorption, and the reaction of adsorbed CO with adsorbed oxygen as well as with subsurface oxygen. Here p_{CO} denotes the CO partial pressure in the gas phase, and the parameter δ describes the effect of O_{ad} on the adsorption rate of CO. The second equation expresses the balance of adsorbed oxygen with contributions to adsorption, to reaction with CO_{ad}, and to formation of subsurface oxygen. The parameter α describes the effect of O_{sub} on the adsorption rate of oxygen, and p_{O_2} is the partial pressure of oxygen in the gas phase. The last equation

accounts for changes in the concentration of subsurface oxygen due to the penetration of adsorbed oxygen into the subsurface region of the palladium bulk, and due to the reaction with adsorbed CO.

Our assumption is that the individual catalytic layers may be considered as spatially homogeneous, because of a strong local coupling inside the layer provided by heat conduction or diffusion of adsorbed species. In the following, we consider the parameter range where the kinetic model equations (1)–(3) exhibit rate oscillations.

We are interested in patterns which appear on a larger scale and focus on the coupling between the catalytic layers in the reactor through variations of the CO partial pressure in the gas phase. Let $p_{\mathrm{CO}}^{\mathrm{i}}$ denote the partial pressure at the inlet of the reactor. For the partial pressure at the first layer, $p_{\mathrm{CO}}^{(1)}$, we have

$$\frac{\mathrm{d}p_{\mathrm{CO}}^{(1)}}{\mathrm{d}t} = \frac{F}{V_{\mathrm{c}}^{(1)}}(p_{\mathrm{CO}}^{\mathrm{i}} - p_{\mathrm{CO}}^{(1)}) - \frac{\mu}{V_{\mathrm{c}}^{(1)}}[k_1 p_{\mathrm{CO}}^{(1)}(1 - u^{(1)} - \delta v^{(1)}) - k_{-1}u^{(1)}], \tag{4}$$

where the upper indices in brackets refer to the number of the layer. F denotes the flow rate through the reactor and μ the coupling strength. $V_{\mathrm{c}}^{(j)}$ is the volume of the catalyst in the jth layer. In between the two layers j and $j+1$, there is neither adsorption nor desorption, therefore

$$\frac{\mathrm{d}p_{\mathrm{CO}}^{m(j)}}{\mathrm{d}t} = \frac{F}{V_{\mathrm{r}}^{m(j)}}(p_{\mathrm{CO}}^{(j)} - p_{\mathrm{CO}}^{m(j)}), \tag{5}$$

where index m labels the CO partial pressure between the two layers. Here, $V_{\mathrm{r}}^{(j)} = d^{(j)}A$ is the volume between layers j and $j+1$, where $d^{(j)}$ and A denote the distance between the layers and the cross-section of the reactor, respectively. An equation analogous to (4) holds for the next layers.

$$\frac{\mathrm{d}p_{\mathrm{CO}}^{(j+1)}}{\mathrm{d}t} = \frac{F}{V_{\mathrm{c}}^{(j+1)}}(p_{\mathrm{CO}}^{m(j)} - p_{\mathrm{CO}}^{(j+1)}) - \frac{\mu}{V_{\mathrm{c}}^{(j+1)}}[k_1 p_{\mathrm{CO}}^{(j+1)}(1 - u^{(j+1)} - \delta v^{(j+1)}) - k_{-1}u^{(j+1)}]. \tag{6}$$

Table 1
Parameter values used in the numerical calculations [21]

Kinetic constants	Further parameter values
$k_1 = 80.0$ (Torr^{-1} s^{-1})	$\alpha = 10.0$
$k_{-1} = 7.545$ (s^{-1})	$\delta = 0.6$
$k_2 = 89.726$ (Torr^{-1} s^{-1})	$\mu = 0.871$ (Torr cm^3)
$k_3 = 282.441$ (s^{-1})	$V_{\mathrm{c}} = 7.7 \times 10^{-4}$ (cm^3)
$k_4 = 0.179$ (s^{-1})	$p_{\mathrm{O}_2} = 152$ (Torr)
$k_5 = 0.053$ (s^{-1})	

For a reactor with only one catalyst layer, Eq. (4) or (6) would describe a global coupling through the gas phase.

We characterize the dynamic regime of the system by the reaction rate and use the flow rate and the partial pressure at the reactor inlet as bifurcation parameters. The reaction rate of the jth layer is

$$R^{(j)} = k_3^{(j)}u^{(j)}v^{(j)} + k_5^{(j)}u^{(j)}w^{(j)}. \tag{7}$$

In the stationary state, instead of (7) we can use the rates (see Eqs. (1) and (4))

$$R^{+(1)} = \frac{F}{\mu}(p_{\mathrm{CO}}^{\mathrm{i}} - p_{\mathrm{CO}}^{(1)}),$$
$$R^{+(j)} = \frac{F}{\mu}(p_{\mathrm{CO}}^{m(j-1)} - p_{\mathrm{CO}}^{(j)}), \quad 1 < j \leq N, \tag{8}$$

which neglect short-time transients.

To study the dynamical consequences of the coupling, we have numerically integrated the model using a Rosenbrock method for stiff sets of differential equations [23]. The bifurcation diagrams are obtained with the CANDYS/QA program developed for numerical bifurcation analysis of non-linear differential equations [24]. The values for the kinetic constants k_i ($i = 1, \ldots, 5$) and the parameters α, δ, μ, V_{c}, and p_{O_2} used during the numerical simulations are given in Table 1 (compare [21]).

3. Results

3.1. Two layers

Numerical simulations of the two-layer system revealed a variety of dynamic regimes. At high flow rates, we find frequency synchronization between the two layers. The partial pressure at the forced

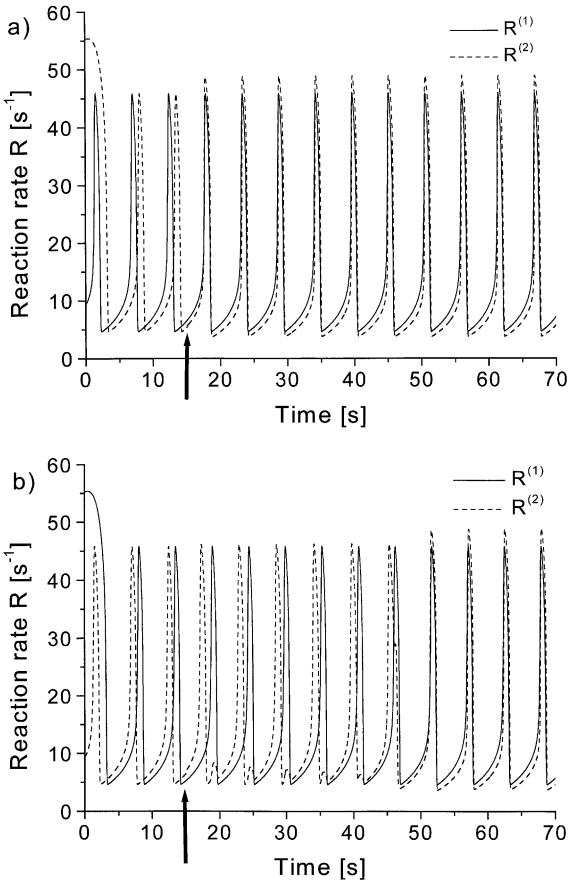

Fig. 2. Fast (a) and slow (b) synchronization in the two-layer system at high flow rates. The reaction rate over the first (full line) and the second layer (broken line) are shown as a function of time. The arrows indicate the time moment when the coupling between the layers is switched on ($p^{i}_{CO} = 2.5\,\text{Torr},\ F = 250\,\text{ml/s},\ V_r = 2\,\text{cm}^3$).

downstream layer $p^{m(1)}_{CO}$ exhibits small amplitude oscillations around a time-independent mean value which is smaller than p^{i}_{CO}. For an uncoupled layer, the frequency of the rate oscillations increases with decreasing CO partial pressure [21]. Under weak coupling, the rate oscillations at the second layer have higher frequency than at the first layer. But for strong coupling at high flow rates, both layers act synchronously with a phase shift $\tau = V_r/F$ that corresponds to the time necessary for the communication between the layers. Synchronized behavior for strong coupling is in accordance with experimental data [25].

When we start with different initial conditions for two identical uncoupled layers, and switch on the coupling at a certain time t_0, then the synchronized regime is reached after a characteristic time interval σ, which depends on the phase shift between the two layers at t_0. For positive phase shift, when the first layer oscillates in advance of the second layer, synchronization takes place rapidly (Fig. 2a), and we obtain values of σ about one or two oscillation periods of the uncoupled system. If at t_0 there is a phase delay between the first and second layer, then the numerical simulations reveal long transients to the synchronized regime (Fig. 2b). In this case of negative phase shift, we have slow instead of fast synchronization, and σ is equal to many oscillation periods.

Usually we find delayed response of the downstream layer (compare Fig. 2 and Fig. 5). However, in a small range of CO partial pressures at the reactor inlet ($4.2\,\text{Torr} \le p^{i}_{CO} \le 6.4\,\text{Torr}$ for $F = 2.5\,\text{ml/s}$, $V_r = 2\,\text{cm}^3$) at first the downstream layer becomes active and the reaction goes through a maximum. Only when the activity at the downstream layer breaks down can the upstream layer become active (Fig. 3). This behavior was not observed for weak coupling in the case of large distances between the layers. Then the downstream layer oscillates at its own frequency. Obviously the flow-mediated coupling is too weak for synchronization (Fig. 4).

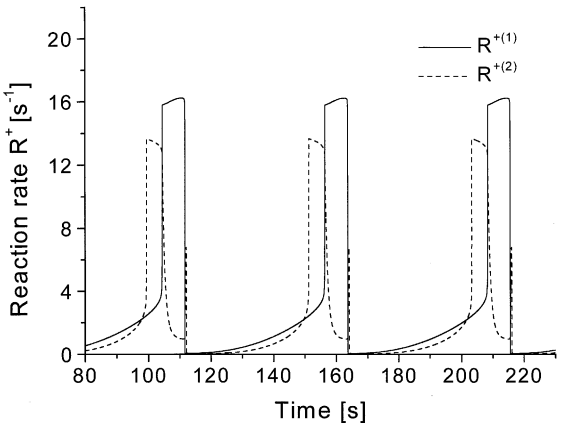

Fig. 3. Advanced response of the downstream layer. The full (broken) line represents the reaction rate over the first (second) layer ($p^{i}_{CO} = 6\,\text{Torr},\ F = 2.5\,\text{ml/s},\ V_r = 2\,\text{cm}^3$).

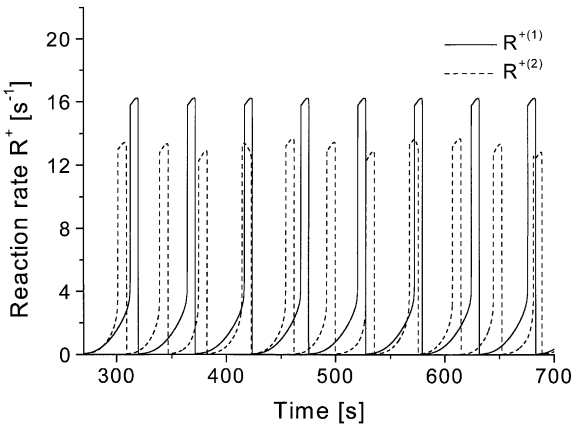

Fig. 4. Breakdown of synchronization for weak coupling for large values of V_r. The full (broken) line represents the reaction rate over the first (second) layer ($p^i_{CO} = 6\,\text{Torr},\ F = 2.5\,\text{ml/s},\ V_r = 200\,\text{cm}^3$).

At low flow rates, we found that a drop in the reaction rate at the first layer can result in a compensating increase of catalytic activity at the second layer (Fig. 5). This phenomenon has been observed experimentally recording the temperature in the layer as a measure for the reaction rate. In Fig. 5, a temperature drop in the first layer is followed by a temperature increase in the second layer.

We have carried out a numerical bifurcation analysis for the coupled two-layer system. Two examples of the bifurcation diagrams are shown in Figs. 6 and 7. Fig. 6 corresponds to a fixed, high flow rate ($F = 250\,\text{ml/s}$). The CO pressure at the reactor inlet is used as bifurcation parameter. As long as p^i_{CO} is small, we have steady-state behavior for both layers. Increasing the p^i_{CO}, the steady state of the system becomes unstable with respect to limit cycle oscillations by a supercritical Hopf-bifurcation (left full square in Fig. 6). This bifurcation can be assigned to the upstream layer, because it occurs in the one-layer model described by Eqs. (1)–(4) as well. The coupling to the downstream layer is irrelevant for this bifurcation. Due to the high flow rate, the periodic variations of $p^{m(1)}_{CO}$ trigger oscillations in the downstream layer. The amplitude of the $p^{m(1)}_{CO}$ oscillations is small, about 2% of the mean value over one oscillation period. Because the mean value is below the threshold for rate oscillations in the second layer, without the periodic input provided by the first layer, the second layer would remain in a steady state. For slightly higher p^i_{CO} values, a second pair of complex-conjugate eigenvalues crosses the imaginary axis changing its real part from negative to positive (open circle in Fig. 6). This behavior occurs only in the coupled two-layer system. Now, with an input equal to the corresponding mean value of the $p^{m(1)}_{CO}$

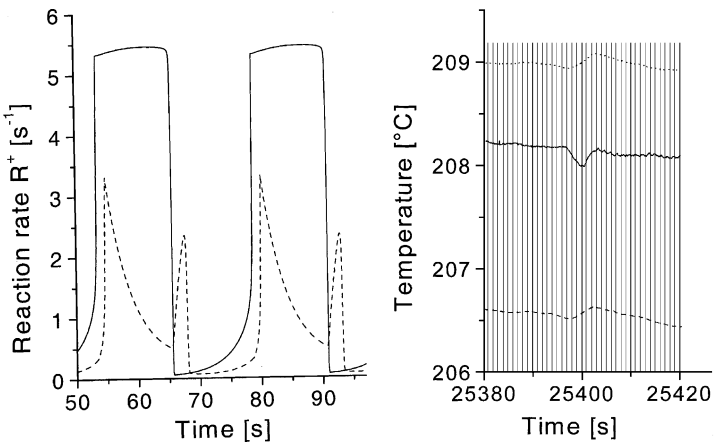

Fig. 5. Activity compensation by the downstream layer. Numerical results (left) have been calculated for $p^i_{CO} = 2\,\text{Torr},\ F = 2.5\,\text{ml s}$, and $V_r = 10\,\text{cm}^3$. The full (broken) line represents the reaction rate over the first (second) layer. Experimental data (right, courtesy of C. Ballandis) obtained for a CO concentration at the inlet of 1.23 vol.%, $F = 75\,\text{ml min}$ and a distance between the layers equal to 1 cm. Full line: temperature at the first layer; dashed and dotted line: temperature at the second layer (two thermoelements in the second layer have been used in the measurements).

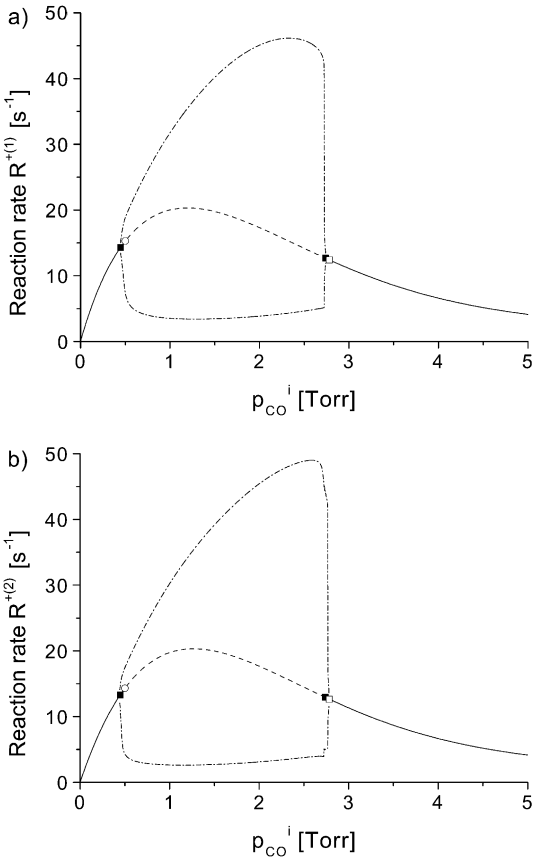

Fig. 6. Bifurcation diagram showing the reaction rates of the upstream (a) and the downstream (b) layer plotted versus the CO partial pressure p^{i}_{CO} for given flow rate $F = 250\,\mathrm{ml\,s}$ ($V_r = 2\,\mathrm{cm}^3$). Full line: stable steady state, dashed line: unstable steady state, dashed-dotted line: oscillation amplitude. Squares refer to Hopf-bifurcations (for explanation see text), open circles correspond to complex-conjugate eigenvalues with vanishing real part in the coupled two-layer system.

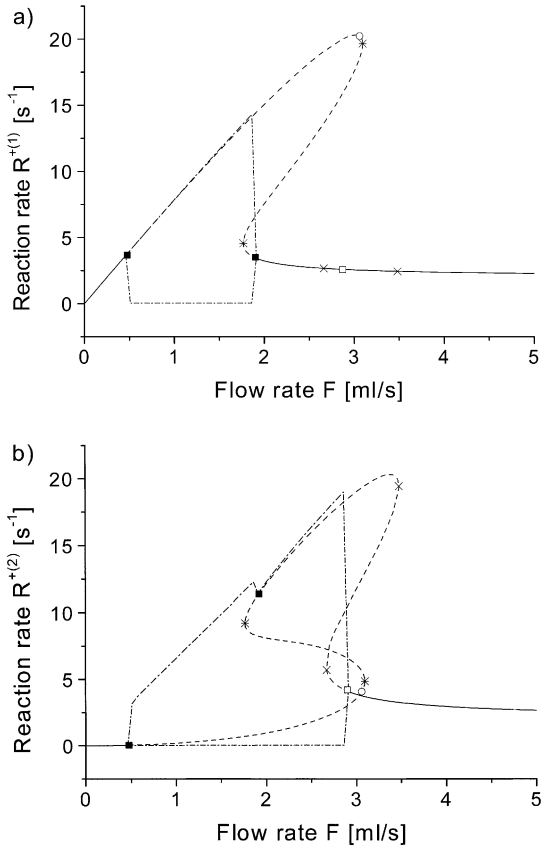

Fig. 7. Bifurcation diagram showing the reaction rates of the upstream (a) and the downstream (b) layer plotted versus the flow rate for given CO partial pressure at the reactor inlet (p^{i}_{CO}=7.0 Torr, $V_r = 2\,\mathrm{cm}^3$). Lines and symbols as in Fig. 6. Additionally, asterisks (crosses) denote saddle-node bifurcations assigned to the one-layer (two-layer) system (compare main text).

oscillations, the second layer displays rate oscillations. Under further increase of p^{i}_{CO}, the oscillations in the first layer terminate by an inverse Hopf-bifurcation, while the second layer still keeps oscillating (right filled square in Fig. 6). But for slightly higher p^{i}_{CO} values, after a second inverse Hopf-bifurcation, both layers are again in the steady state. The second inverse Hopf-bifurcation occurs only in the coupled two-layer system (open square in Fig. 6). Because of the high flow rate, the upstream and the downstream layer act almost synchronously, and therefore there is no qualitative difference between Fig. 6a and b. The bifurcation diagram in Fig. 6 is very similar to that of the one-layer system [21].

However, the bifurcation diagram of the two-layer system can be more complicated, as follows from Fig. 7. Here the flow rate is used as bifurcation parameter. In the case of intermediate p^{i}_{CO}-values ($p^{i}_{CO} =$ 7 Torr), both layers are in a steady state, when F is small. With increasing F, the first Hopf-bifurcation occurs (left filled square in Fig. 7). In an extended range of flow rates, the oscillations in the first layer trigger oscillations in the second layer. The oscillation amplitude of the partial pressure $p^{m(1)}_{CO}$ is large, about 50%

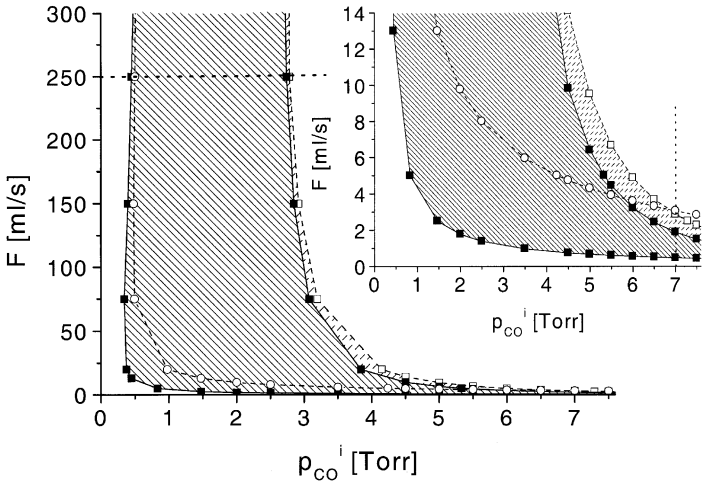

Fig. 8. Bifurcation map in the p^{i}_{CO} versus F plane showing the modes of operation for the two-layer reactor ($V_r = 2\,cm^3$). White domains: steady-state behavior; full-hatched domain: rate oscillations in the upstream layer force rate oscillations in the downstream layer; broken-hatched domain: the upstream layer is in the steady state, while the downstream layer exhibits rate oscillations. Symbols as in Figs. 6 and 7. The bifurcation diagram in Fig. 6 (Fig. 7) corresponds to a section along the horizontal (vertical) broken line.

of the mean value over one period of oscillation. Under these conditions, we observe advanced and compensating response as discussed above (compare Figs. 3 and 5, respectively). Further increase of the flow rate results in a saddle-node bifurcation of the unstable steady state of the first layer without any consequences for the operation mode of the reactor. The next bifurcation with increasing F is an inverse Hopf-bifurcation terminating the rate oscillations in the first layer (right filled square in Fig. 7). Now, the output of the first layer is constant in time, but for the corresponding constant value of $p^{m(1)}_{CO}$, the second layer still keeps oscillating. After a saddle-node bifurcation of the unstable branch not associated with the formation of stable regimes, oscillations of the second layer disappear by an inverse Hopf-bifurcation (open square in Fig. 7). At higher F values, the real part of a pair of complex-conjugate eigenvalues changes its sign from positive to negative (open circle in Fig. 7), and a saddle-node bifurcation referring to unstable states occurs. However, the system remains in the steady state.

The results of the numerical bifurcation analysis are summarized in Fig. 8, which depicts the stable dynamic regimes in the parameter plane spanned by p^{i}_{CO} and F. We find an extended parameter region, where rate oscillations at the upstream layer trigger rate oscillations at the downstream layer. Two separated regions with steady-state behavior of the coupled system exist. The first is located in the lower left corner of the parameter plane and close to the two coordinate axes, where either p^{i}_{CO}, F or both are small. Here, the steady state becomes unstable with respect to sustained oscillations of the first layer. These oscillations trigger oscillatory behavior at the downstream layer. For the second region, characterized by larger p^{i}_{CO} values, the instability of the steady state occurs via oscillations of the second layer. The first layer remains in the steady state.

3.2. N layers

The numerical simulations have been extended towards the case of many layers. As in the two-layer system, we find synchronization of all layers, when the flow rate is sufficiently high (strong coupling). Lowering the flow rate, the layers far from the reactor inlet display compensated behavior, while the layers near to the reactor inlet still act synchronously. The shape of the rate oscillation changes accordingly, compare Fig. 9, where one period of the rate oscillations at five different layers in a reactor with altogether 30 layers is shown.

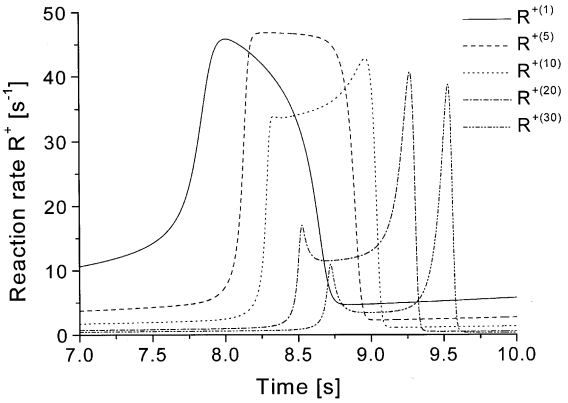

Fig. 9. Rate oscillations at different layers in a 30-layer reactor at large flow rates. For all chosen layers, only one oscillation period is shown ($p^{i}_{CO} = 2.5\,\text{Torr}$, $F = 250\,\text{ml/s}$, $V_r^{m(j)} = 5\,\text{cm}^3$).

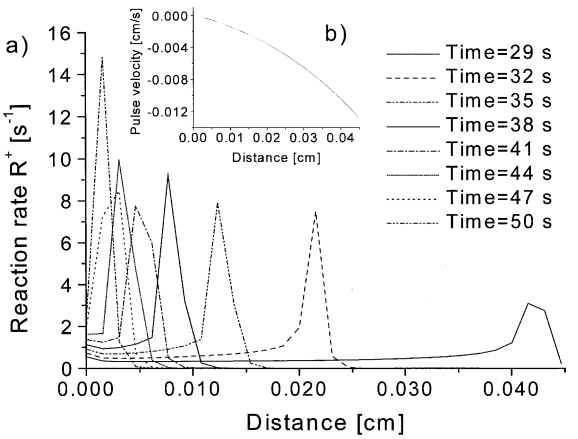

Fig. 11. (a) Upstream moving pulses in a 30-layer reactor ($p^{i}_{CO} = 6.4\,\text{Torr}$, $F = 2.5\,\text{ml/s}$, $V_r = V_c = 7.7 \times 10^{-4}\,\text{cm}^3$). (b) Pulse velocity over the distance from the reactor inlet. Same initial condition as for Fig. 10a.

Of interest is the case of large N with small volume between the layers, which approximates a fixed-bed reactor. In the following, we equate the volume of the catalyst in the layer with the volume between two layers, $V_c = V_r$. Fig. 10a presents the reaction rate over the reactor length for the case of 100 layers. Sequences of downstream moving activity pulses propagate through the reactor, provided the flow rate exceeds a certain threshold F_{cr} which is close to the threshold for the excitation of sustained oscillations in the layer at the reactor inlet. Fig. 10b displays the propagation velocity of the pulse versus the distance from the reactor inlet. After some transient, the velocity remains constant. In the parameter range with advanced response (Fig. 3), upstream moving pulses are possible with a velocity, which is going to be smaller with decreasing distance to the inlet (Fig. 11a

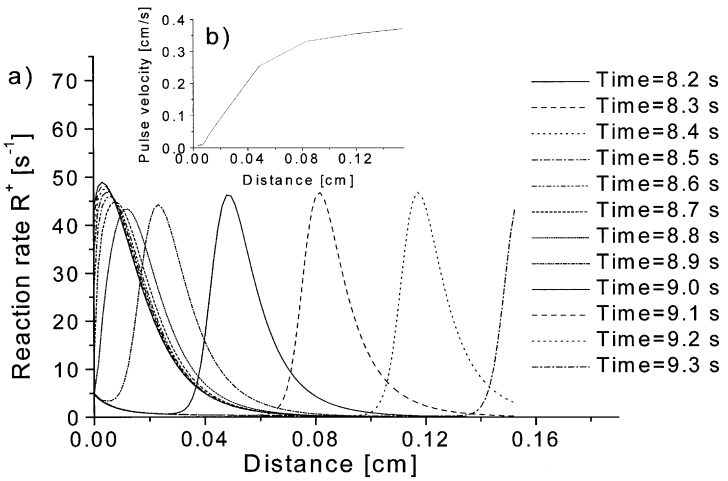

Fig. 10. (a) Spontaneously formed activity pulses propagating downstream in a 100-layer reactor. Numerical simulations start at zero time with spatially uniform initial conditions ($p^{i}_{CO} = 2.5\,\text{Torr}$, $F = 250\,\text{ml/s}$, $V_r = V_c = 7.7 \times 10^{-4}\,\text{cm}^3$). (b) Pulse velocity over the distance from the reactor inlet.

and b). These pulses correspond to kinematic or phase waves in oscillatory media.

4. Discussion

We have modeled the CO oxidation in a flow reactor containing N layers of zeolite-supported palladium. The model focuses on the effect of flow-mediated spatial coupling between the layers provided by CO partial pressure variations transmitted by the flow. Each layer is assumed to behave spatially uniform due to a strong local coupling provided by diffusion or heat conduction. The corresponding terms in the balance equations (1)–(3) are omitted. In this limit, each catalytic layer is represented by a non-linear oscillator.

By numerical simulations, we have analyzed the effect of different flow rates and CO partial pressure at the reactor inlet on the dynamics of the reactor. Depending on these parameters, we find a large variety of dynamic regimes including synchronization at large flow rates, delayed and advanced response of downstream layers, the so-called compensation regime, and propagating pulses of catalytic activity. During the calculations, realistic values for the parameters have been used. Some of the numerical results for the two-layer system agree with experimental data obtained in a tube reactor with two zeolite-supported palladium layers on Teflon disks [25]. To get a better understanding of the dynamics for the two-layer system, we have performed a numerical bifurcation analysis using the CO partial pressure at the reactor inlet and the flow rate as bifurcation parameters.

We suppose that our main results do not depend on the specific kinetics described by the particular equations (1)–(3). Any model with relaxational oscillations is expected to lead to qualitatively equivalent results, when a coupling according to Eqs. (4)–(6) is considered.

The model allows to study other effects, as non-uniformity in the parameters leading to different properties of the individual catalytic layers, synchronization phenomena under periodic modulations of the CO partial pressure at the reactor inlet, and the impact of variations in the distance between the layers. For a more realistic description of catalytic reactions under normal pressure, the balance of energy and the temperature dependence of the rate constants must be included into the model. However, these investigations are beyond the scope of this paper.

Acknowledgements

We have benefited much from discussions with M. Slin'ko, N. Jaeger, and P. Plath. Financial support by the VW-Stiftung (project 70603) is gratefully acknowledged.

References

[1] M.C. Cross, P.C. Hohenberg, Pattern formation outside of equilibrium, Rev. Mod. Phys. 65 (1993) 851.
[2] G. Ertl, Oscillatory kinetics and spatio-temporal self-organization in reactions at solid surfaces, Science 254 (1991) 1750.
[3] S. Jakubith, H.H. Rotermund, W. Engel, A. von Oertzen, G. Ertl, PRL 65 (1990) 3013.
[4] M. Sheintuch, S. Shvartsman, AIChE J. 42 (1996) 1041.
[5] M.M. Slin'ko, N.I. Jaeger, Oscillatory Heterogeneous Catalytic Systems: Studies in Surface Sciences and Catalysis, Vol. 86, Elsevier, Amsterdam, 1994.
[6] D. Luss, Ind. Eng. Chem. Res. 36 (1997) 2931.
[7] R. Kapral, K. Showalter (Eds.), Chemical Waves and Patterns, Kluwer Academic Publishers, Dordrecht, 1995.
[8] M. Falcke, H. Engel, J. Chem. Phys. 101 (1994) 6255.
[9] M. Falcke, H. Engel, M. Neufeld, Phys. Rev. E 52 (1995) 763.
[10] M. Falcke, H. Engel, Phys. Rev. E 56 (1997) 635.
[11] D. Battogtokh, A.S. Mikhailov, Physica D 90 (1996) 84.
[12] D. Battogtokh, M. Hildebrand, K. Krischer, A.S. Mikhailov, Phys. Rep. 288 (1997) 235.
[13] F. Mertens, R. Imbihl, A.S. Mikhailov, J. Chem. Phys. 101 (1994) 9903.
[14] D. Battogtokh, A. Preusser, A.S. Mikhailov, Physica D 106 (1997) 327.
[15] M. Bertram, A.S. Mikhailov, Pattern formation in a surface chemical reaction with global delayed feedback, Preprint, 2001.
[16] A.B. Rovinsky, M. Menzinger, Phys. Rev. Lett. 69 (1992) 1193.
[17] A.B. Rovinsky, M. Menzinger, Phys. Rev. Lett. 70 (1993) 778.
[18] N.I. Jaeger, K. Möller, P.J. Plath, J. Chem. Soc., Faraday Trans. 82 (1986) 3315–3330.
[19] M.R. Bassett, R. Imbihl, J. Chem. Phys. 93 (1990) 811–821.

[20] M. Liauw, P.J. Plath, N.I. Jaeger, J. Chem. Phys. 104 (1996) 6375–6386.
[21] M.M. Slin'ko, E.S. Kurkina, M. Liauw, N.I. Jaeger, J. Chem. Phys. 111 (1999) 8105–8114.
[22] M.M. Slin'ko, A.A. Ukharskii, N.I. Jaeger, Phys. Chem. Chem. Phys. 3 (2001) 1015–8114.
[23] W.H. Press, S.A. Teukolsky, W.T. Vetterling, B.P. Flannery, Numerical Recipes in C, Cambridge University Press, Cambridge, 1992.
[24] U. Feudel, W. Jansen, CANDYS/QA — a software system for the qualitative analysis of nonlinear dynamical systems, Int. J. Bifurc. Chaos 2 (1992) 773–794.
[25] C. Ballandis, Unpublished results.